

The Moderate Impact of the 2015 El Niño over East Africa and Its Representation in Seasonal Reforecasts

DAVID MACLEOD

Atmospheric, Oceanic and Planetary Physics, University of Oxford, Oxford, United Kingdom

CYRIL CAMINADE

Institute of Infection and Global Health, Department of Epidemiology and Population Health, University of Liverpool, Liverpool, United Kingdom

(Manuscript received 13 March 2019, in final form 13 August 2019)

ABSTRACT

El Niño–Southern Oscillation (ENSO) has large socioeconomic impacts worldwide. The positive phase of ENSO, El Niño, has been linked to intense rainfall over East Africa during the short rains season (October–December). However, we show here that during the extremely strong 2015 El Niño the precipitation anomaly over most of East Africa during the short rains season was less intense than experienced during previous El Niños, linked to less intense easterlies over the Indian Ocean. This moderate impact was not indicated by reforecasts from the ECMWF operational seasonal forecasting system, SEAS5, which instead forecast large probabilities of an extreme wet signal, with stronger easterly anomalies over the surface of the Indian Ocean and a colder eastern Indian Ocean/western Pacific than was observed. To confirm the relationship of the eastern Indian Ocean to East African rainfall in the forecast for 2015, atmospheric relaxation experiments are carried out that constrain the east Indian Ocean lower troposphere to reanalysis. By doing so the strong wet forecast signal is reduced. These results raise the possibility that link between ENSO and Indian Ocean dipole events is too strong in the ECMWF dynamical seasonal forecast system and that model predictions for the East African short rains rainfall during strong El Niño events may have a bias toward high probabilities of wet conditions.


1. Introduction


Extreme climate hazards are associated with El Niño events and 2015/16 saw one of the strongest events ever recorded (Huang et al. 2016). El Niño is the warm phase of El Niño–Southern Oscillation (ENSO), and strong events significantly disturb the Walker cell zonal circulation over the tropics, changing the likelihood of regional drought and flooding across the globe (Vicente-Serrano et al. 2011; Emerton et al. 2017).

More precisely, the disturbance of circulation patterns induced by El Niño significantly reduces rainfall in

Australia, Indonesia, and Brazil while increasing rainfall over western coastal and southern South America, southern China, eastern Africa, and the southern United States during the boreal winter season (Mason and Goddard 2001). Its impacts are milder during boreal summer, with increased drought conditions observed over India, Australia, and Central America (McPhaden et al. 2006). The largest El Niño events (such as the 1997/98 and 2015/16 events) tend to have the largest impacts on socioeconomic factors and the health of population in the tropics, whereas the impacts of weak El Niño events, (such as the 2004/05 event) are difficult to distinguish from atmospheric background noise (McPhaden et al. 2006).

The impacts of El Niño on regional rainfall and temperature cascade into significant impacts on agriculture, weather extremes, socioeconomic factors, and human

 Denotes content that is immediately available upon publication as open access.

 Supplemental information related to this paper is available at the Journals Online website: <https://doi.org/10.1175/JCLI-D-19-0201.s1>.

Corresponding author: David MacLeod, macleod@atm.ox.ac.uk

DOI: 10.1175/JCLI-D-19-0201.1

© 2019 American Meteorological Society



This article is licensed under a [Creative Commons Attribution 4.0 license](http://creativecommons.org/licenses/by/4.0/) (<http://creativecommons.org/licenses/by/4.0/>).

and animal health (Kovats et al. 2003; McGregor and Ebi 2018; Anyamba et al. 2019). During El Niño 2015/16, several catastrophic events took place, such as droughts and increased bleaching of coral reefs in Australia and Indonesia, droughts depleting livestock numbers and affecting crops in Ethiopia and South Africa, and large forest fires affecting Malaysia, Indonesia, and neighboring countries (Claar et al. 2018; International Federation of Red Cross and Red Crescent Societies 2017; Field et al. 2016). El Niño has also been associated with the emergence and re-emergence of infectious diseases in the tropics (Hales et al. 1999; Chretien et al. 2015; McGregor and Ebi 2018).

Large outbreaks of Rift Valley Fever, malaria, and cholera over East Africa during the short rains season, increased transmission of dengue and malaria in Latin America and Southeast Asia during and following the South American and Asian monsoons, and outbreaks of malaria and cholera in India during the Indian monsoon and summer seasons have been reported during large El Niño events (Anyamba et al. 2019). The recent Zika virus outbreak that plagued Latin America from early 2015 to November 2016 and spread to other countries in Africa and Southeast Asia was also favored by regional climate anomalies induced by El Niño (Caminade et al. 2017; Muñoz et al. 2017; Sorensen et al. 2017).

The strong correlation between the East African short rains [October–December (OND)] and ENSO is well known (Hastenrath et al. 1993; Indeje et al. 2000; Wolff et al. 2011): significant widespread seasonal rainfall anomalies tend to occur during El Niño events, leading to increased risk of flooding. This was particularly the case during OND 1997 (Nicholson 2017). A clear fingerprint of strong El Niño events can also be seen on population health in the region: during the 1958/59 El Niño, abnormally high temperature, rainfall, and relative humidity resulted in 3 million malaria cases over the highlands of Ethiopia (Fontaine et al. 1961), whereas during the 1997/98 event higher temperatures and increased precipitation also resulted in increased malaria prevalence in Kenya (Brown et al. 1998; Omumbo et al. 2011) and Uganda (Kilian et al. 1999).

ENSO is understood to influence the short rains over East Africa through the modulation of the Walker-type coupled zonal circulation in the central equatorial Indian Ocean (Mutai and Ward 2000; Hastenrath et al. 2011). Normal conditions consist of prevailing surface westerlies over the Indian Ocean, easterly flow at 200 mb (1 mb = 1 hPa), rising motion in the east, and subsidence over the far west Indian Ocean, suppressing rainfall over East Africa. Note that this subsidence cap is at least partly responsible for the unusual occurrence of a semiarid climate

on the equator. Circulation changes induced by El Niño then lead to zonal wind anomalies over the Indian Ocean of an opposite sign to the mean flow, at height (200 mb) and near the surface (850 mb), corresponding to a weakening of the Walker-type circulation, a reduction of the subsidence cap over East Africa, and increased rainfall. In addition to ENSO, the Indian Ocean dipole (IOD; Saji et al. 1999) exerts a strong control on the East African short rains (Nicholson 2017) through the same pathway as ENSO with positive events leading to weakening and potentially reversal of the Walker-type circulation over the Indian Ocean.

During the 2015 short rains, El Niño was at its peak. Seasonal forecast models had well anticipated the onset and strength of the event, with public advisories issued during the first half of 2015 (L'Heureux et al. 2017). Based on warnings of a strong El Niño event alone, the humanitarian sector conducted preparedness actions for an extreme wet season in East Africa, basing actions on the impacts of similar intensity El Niño events (Tozier de la Poterie et al. 2018).

However in the event, although some parts of East Africa experienced a particularly wet season, for many other parts (eastern and central Kenya, parts of Somalia) the wet anomaly was not particularly strong; and parts of Ethiopia, Somalia, and Tanzania even experienced a drier than average season. Despite the fact that the season coincided with one the largest El Niño events on record, the rainfall impact over East Africa was much less spatially coherent and of lower magnitude compared to impacts during the 1997 event, when the El Niño index was slightly lower than 2015.

The impact of El Niño 2015/16 over the western United States was also unexpected and significant attention has been paid to this event over this region. Here the boreal winter precipitation was much lower than expected from the impact of previous strong El Niño events, and seasonal forecasts performed poorly for this event (Wanders et al. 2017). Several studies have examined reasons for this and suggest that internal variability played a significant role (Zhang et al. 2018; Cash and Burls 2019; Lim et al. 2018), while other work found that the weak precipitation in 2015/16 relative to previous major events was likely related to a pattern of tropical SST variability outside of the El Niño core region (Quan et al. 2018), largely arising from the Indian Ocean and western Pacific (Siler et al. 2017).

Little attention has been paid to the details of the impact of the 2015 El Niño over East Africa. However, in order to evaluate the reliability of future El Niño-related early warnings it is essential to understand the reasons behind the unexpectedly moderate impact of this particular event in the region, when compared to the

impact of historical El Niños. We address this question here through analysis of climate observations and reanalysis. To understand the potential of forecasting systems to anticipate 2015 conditions we evaluate dynamical seasonal reforecasts of the season. These reveal high probability forecasts for a particularly wet season to occur, despite the observed dry conditions. To diagnose the reasons for this strong signal we describe the results of some atmospheric relaxation experiments. This experimental technique and other methods are described in the following section, which also contains details of the observations and model datasets. Results and discussions follow in [sections 3 and 4](#).

2. Data and methods

a. Observational data

The Climate Hazards Infrared Precipitation with Stations (CHIRPS; [Funk et al. 2015](#)) is used for analysis of precipitation and verification of seasonal reforecasts. CHIRPS is a blend of station and satellite data, providing daily precipitation estimates at $0.05^\circ \times 0.05^\circ$ spatial resolution from 1981 to the present. For analysis where precipitation over the ocean is considered, the Global Precipitation Climatology Project (GPCP) dataset is used ([Adler et al. 2003](#)), which is a monthly precipitation dataset combining satellite and observations on a $2.5^\circ \times 2.5^\circ$ grid. Sea surface temperatures are derived from the HadISST dataset ([Rayner et al. 2003](#)). Dynamic fields to characterize the near-surface circulation (winds, velocity potential, and divergent component of winds at 850 mb) were derived from the ERA-Interim reanalysis dataset ([Dee et al. 2011](#)). When comparing to model data, all data are interpolated to a $1^\circ \times 1^\circ$ grid before analysis.

The Niño-3.4 index is used to characterize ENSO; this index is calculated using the averaged SST anomaly for 5°S – 5°N , 170° – 120°W based on HadISST data. The dipole mode index (DMI) is also used in order to characterize the IOD. This is defined as the difference between the average SST in the region 50° – 70°E and 10°S – 10°N minus the average SST in the box 90° – 110°E and 10°S – 0°N . Both the Niño-3.4 and IOD indices were downloaded from the NOAA website (<https://www.esrl.noaa.gov/psd/data/climateindices/list/>). All analysis has been calculated for OND, corresponding to the short rains season across most of East Africa.

b. Regression and composite analysis on observational data

To explore the relationship between ENSO, the IOD, rainfall, SST, and dynamical variables, linear regression

coefficients were calculated and compared to anomalies. Anomalies are defined as the departure of each climate variable from its seasonal mean state over 1981–2016. Standardized Niño-3.4 and IOD indices were linearly regressed against detrended climate variables (rainfall, SSTs, velocity potential, and the divergent component of the wind at 850 mb) for OND over the period 1981–2016. The resulting linear regression coefficients, representing the average response of the atmosphere to ENSO and the IOD, were then compared to climate anomalies for the three largest El Niño events occurring during the period considered here: 1982, 1997, and 2015. Note that composites of climate anomalies on El Niño and La Niña years reveal patterns of similar shape but opposite sign (not shown), indicating that the linearity assumption underlying regression analysis is appropriate.

c. Seasonal forecast data

Seasonal reforecast data from the European Centre for Medium-Range Weather Forecast (ECMWF) and the Met Office are analyzed in this study, using the forecasts of OND from September start dates across the common reforecast period 1993–2015. Data were retrieved from the Copernicus Data Store (<https://climate.copernicus.eu/seasonal-forecasts>).

The ECMWF operational seasonal forecast, SEAS5, comprises the Integrated Forecasting System (IFS), an atmospheric model, cycle CY43R1, at Tco319 spatial resolution (about $35\text{ km} \times 35\text{ km}$ at the equator), with 91 vertical levels, reaching up to 0.01 mb, to an altitude of about 80 km. IFS is coupled to the Nucleus for European Modeling of the Ocean (NEMO) ocean model v3.4 on a tripolar 0.25° ORCA grid with 75 vertical levels. Ensemble members are perturbed to account for initial condition and model uncertainty, and 25 ensemble members are available for the reforecast.

The Met Office seasonal forecasting system is GloSea5, which is a coupled model based on the MetUM atmospheric model, the JULES land surface model, the NEMO ocean model, and the Los Alamos sea ice model ([MacLachlan et al. 2015](#)). The atmospheric model has spatial resolution of 0.83° (longitude) \times 0.56° (latitude), with 85 levels in the atmosphere and a top at 85 km. The spatial resolution of NEMO is 0.25° on a tripolar ORCA grid, with 75 vertical levels. A total of 28 perturbed ensemble members are available in the reforecast.

d. Atmospheric relaxation experiments

Analysis of SEAS5 forecast reveals high forecast probabilities for a very wet season over East Africa (see [section 3](#)). To explore the mechanisms responsible for such a wet signal, relaxation experiments are carried out. These follow the technique described in [Jung \(2011\)](#),

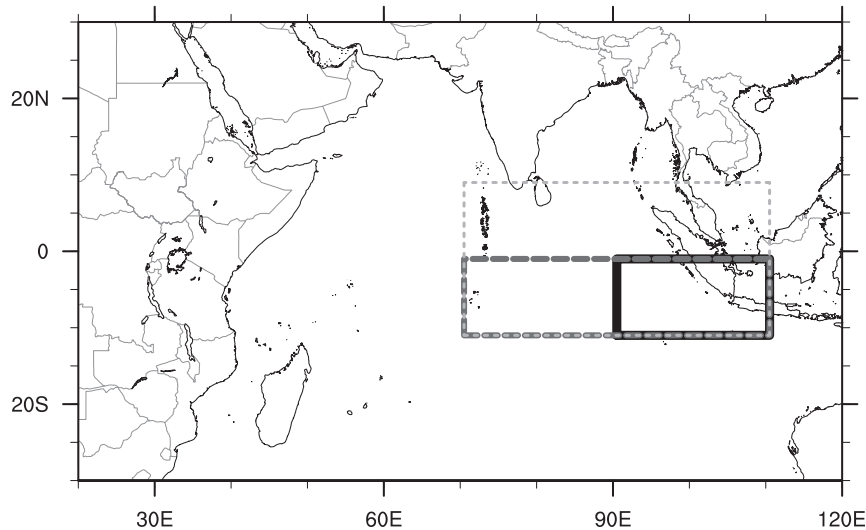


FIG. 1. Regions used for the atmospheric relaxation experiments. The three experiments IOD2, IOD2+, and IOD2++ are shown with the thick black, medium dashed dark gray, and thin dashed light gray lines, respectively.

where the atmosphere is nudged back toward observations (in this case ERA-Interim) at every time step, inside a specified region. Outside of the region the coupled modeling system is allowed to evolve freely. Note that the current study differs from Jung (2011) in that the method is applied to a coupled atmosphere–ocean model, rather than an atmosphere-only model.

The control simulation is a 25-member, 4-month reforecast initialized on 1 September, using the ECMWF-IFS atmosphere model coupled to the NEMO ocean model and initialized with ERA-Interim atmospheric reanalyses and ORAS4 oceanic reanalysis. The resolution of the atmospheric model for the relaxation experiments is T255, cycle CY41R1 (note that this differs from SEAS5 resolution and cycle, which is currently too computationally expensive to use in research mode; however, the forecast for 2015 in the experimental control is similar to that seen in the SEAS5 reforecast).

A series of 25 members' relaxation experiments were then performed. These follow the control setup, but where remote regions are relaxed toward ERA-Interim. Regions in the eastern Indian Ocean were chosen based on differences between the 2015 and 1997 event seen in analysis of reanalysis and reforecasts, presented later. The regions are shown in Fig. 1. The first corresponds to the eastern box used to define the IOD index, 90°–110°E, 0°–10°S (experiment IOD2 hereafter). Extending westward from this box, the second region used was 70°–110°E, 0°–10°S (IOD2+). Finally, a third region extended northward of the equator, covering 70°–110°E, 10°N–10°S (experiment IOD2++). In each case, zonal and meridional wind, humidity, and temperature at

atmospheric levels below 700 mb were relaxed back toward ERA-Interim on a 6-h time step, with logarithmic spatial smoothing at the domain boundaries in order to avoid discontinuities.

3. Results

a. Impacts of the 2015 El Niño on East Africa short rains

Figure 2 shows rainfall during the three highest El Niño years since 1981 according to CHIRPS precipitation data over East Africa, showing the ranking of the year at each point (Figs. 2a–c) as well as standardized rainfall anomalies (Figs. 2d–f). During the 1997 event, the region experienced one of the largest precipitation anomalies on record, with significant parts of Kenya, Somalia, and Ethiopia showing wet anomalies three standard deviations above the mean (Fig. 2e). The year 1982 saw a weaker El Niño, although most of the region experienced rainfall anomalies one standard deviation above the mean, and parts of southern Kenya saw the wettest season on record (Fig. 2d). During 2015, rainfall was much lower than seen in previous El Niños (Fig. 2f); over the Mandera triangle region where Kenya, Somalia, and Ethiopia meet, the anomalies were close to the climatological mean. Uganda experienced the wettest season on record and central Somalia saw a high precipitation anomaly, while drier than average conditions were observed over Somalia, Ethiopia, and Tanzania.

Rainfall anomalies in 2015 were much lower and less spatially coherent than in 1997. Given that the IOD has

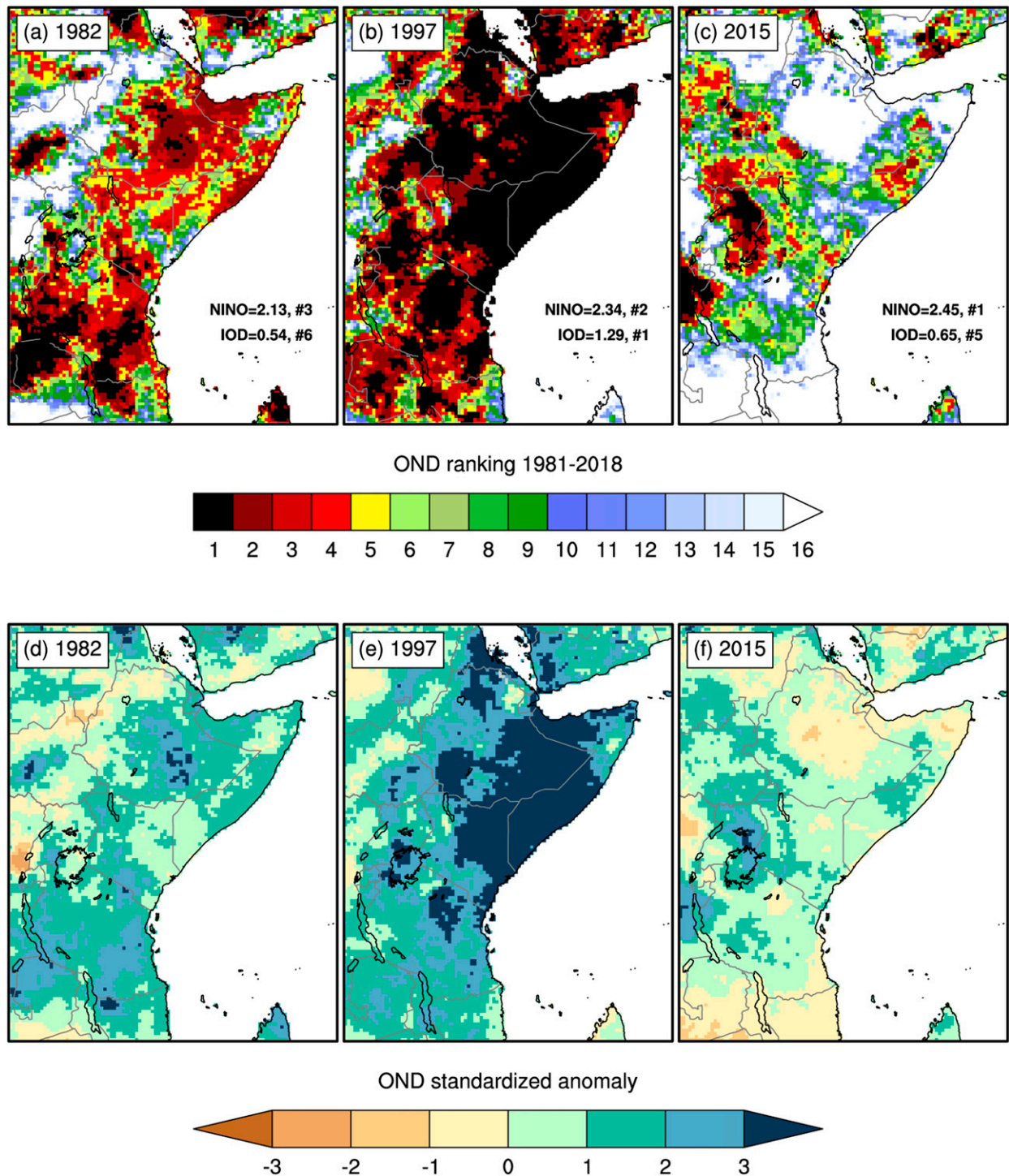


FIG. 2. OND rainfall from CHIRPS during three strong El Niño years, (a) 1982, (b) 1997, and (c) 2015, showing the ranking across 1981–2018 (a ranking of 1 indicates the year was the wettest in the record). (d)–(f) The standardized rainfall anomalies for these seasons. The rank and magnitude of the season mean Niño-3.4 and IOD index are also shown in (a)–(c).

been shown to be a key driver of the East African short rains (Black et al. 2003; Black 2005), it is possible that this phenomenon played a role in the difference between 2015 and 1997 impacts. Indeed, the strongest IOD

on record occurred in 1997, with an index over twice the magnitude as observed in 1982 and 2015 (Figs. 2a–c, inset). To evaluate the relative influence of ENSO and IOD on East African climate, we compare the average

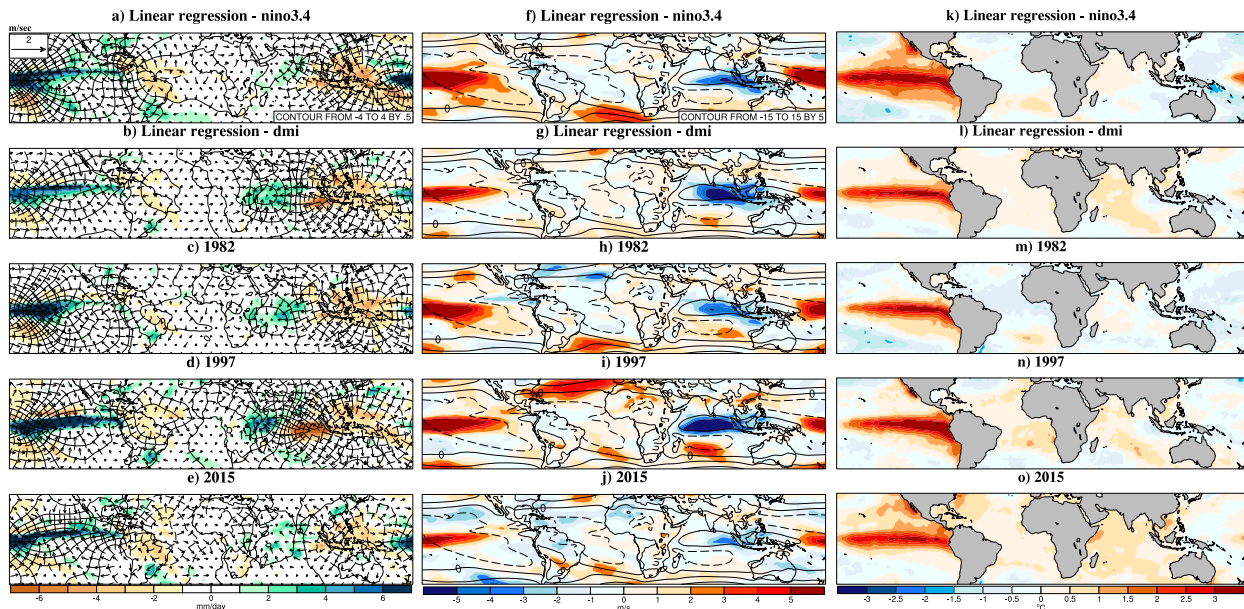


FIG. 3. Comparison of different climate variables regressed over 1981–2016 against the (a),(f),(k) Niño-3.4 index and (b),(g),(l) IOD, with the specific climate anomalies corresponding to (c),(h),(m) 1982, (d),(i),(n) 1997, and (e),(j),(o) 2015. (left) Rainfall (color; mm day^{-1}) and divergent component of the wind at 850 mb (vectors; m s^{-1}). Contours of positive and negative velocity potential at 850 mb are shown in steps of $0.5 \times 10^6 \text{ m}^2 \text{ s}^{-1}$ as solid and dashed lines, with zero indicated by the thicker black contour. (center) The zonal wind anomaly at 850 mb and climatological mean with colors and contours respectively; contours indicate an interval of 5 m s^{-1} ; solid (dashed) indicates positive (negative), with the thicker line indicating the zero contour. (right) SST ($^{\circ}\text{C}$). Note that linear regression coefficients were multiplied by an (arbitrary) factor of 3 to allow visual comparison with the anomalies.

impact of ENSO and IOD on dynamic variables and precipitation in the tropics.

The average impact of ENSO and the IOD is estimated using linear regression and compared to the observed anomalies for 1982, 1997, and 2015; results are shown in Fig. 3. Positive phases of both ENSO and the IOD are associated with increased low-level easterly zonal wind anomalies at 850 mb over the Indian Ocean (Figs. 3f,g), increased surface divergence and drought conditions over Indonesia/Malaysia and Brazil, and increased convergence and consequently increased rainfall conditions over East Africa (Figs. 3a,b). However, the strength of this relationship with the IOD is much stronger than with ENSO, with much stronger easterly wind anomalies, reaching farther into the west of the Indian Ocean and the eastern coasts of Africa. Consistently, the average response to the IOD index indicates larger positive rainfall anomalies over East Africa (Fig. 3b) compared to ENSO (Fig. 3a). This indicates that while both ENSO and IOD are associated with a reversal of the Indian Ocean Walker cell, the impacts of the IOD on East African climate tend to be larger. This finding is consistent with previous work (Nicholson 2017). For reference, the regression of climate fields onto an East Africa OND precipitation index (see Fig. S1 in the online supplemental material) confirms the

strong association between OND rainfall and the zonal wind pattern associated with the IOD.

The 1997 event projects both on positive phases of ENSO and IOD (Figs. 3d,i,n) and is consistently associated with much stronger easterly wind anomalies over the Indian Ocean (Fig. 3i), and consequently larger rainfall anomalies over the western part of the Indian Ocean and East Africa (Fig. 3d). Regional climate anomalies related to the 1982 (Figs. 3c,h,m) and 2015 events (Figs. 3e,j,o) tend to be in closer agreement with regression patterns calculated using the Niño-3.4 index (Figs. 3a,e,j), with weaker easterly wind anomalies over the Indian Ocean and more moderate rainfall anomalies reaching the coasts of East Africa. These results suggest that the moderate impact of the 2015 El Niño on East African rainfall compared to 1997 is linked to weaker IOD-like activity in the Indian Ocean, with no strong cold SST in the east and weaker easterly wind anomalies at 850 mb crossing the Indian basin. With this understanding of the differences between the 2015 event and the canonical El Niño response, we turn to the representation of this event in operational seasonal forecasts.

b. Seasonal forecasts of the 2015 short rains

The consensus seasonal outlook from the Greater Horn of Africa Regional Outlook Forum (GHACOF) is

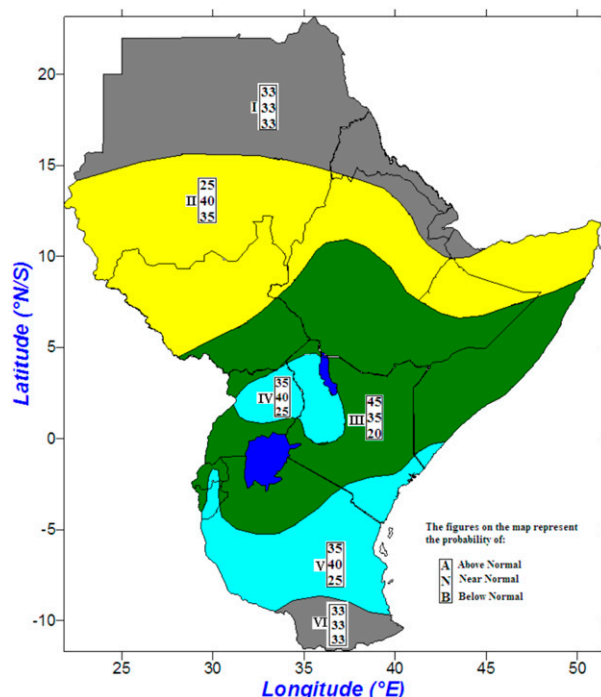


FIG. 4. Consensus forecast from GHACOF41, held in preparation for the short rains (OND) 2015 (ICPAC 2015).

shown in Fig. 4. This forecast was issued at the 41st GHACOF meeting held in August 2015 in Dar es Salaam, Tanzania, just two months before the start of the short rains. At that time the evolution toward a strong El Niño was clearly indicated across all dynamical models (L'Heureux et al. 2017). The consensus rainfall outlook indicated that a probability of 45% was given for upper tercile rainfall over a large region covering most of Kenya and the Mandera triangle, which ultimately did not experience such significant flooding. Note that a probability of 45% is at the top of the range of increased probabilities issued at the GHACOF meeting, which tend to be conservative; see Mason and Simbarashe (2009) for further assessment of the issued probabilities and reliability of Regional Climate Outlook Forum. This outlook is based on a consensus of multiple information streams: forecasts issued by national East African meteorological centers, in-house statistical models, the analog year approach, and dynamical forecasts issued by the WMO-designated Global Producing Centres (GPCs; see <https://www.wmolc.org/> for further details).

The evolution of a strong El Niño in 2015 was anticipated months in advance, in both the ECMWF and the Met Office operational seasonal forecast systems SEAS5 and GloSea5 (Ineson et al. 2018). Figure 5 shows the precipitation anomaly forecast for East Africa for these two forecasting systems at a 1-month lead time for

OND (forecast initialized in September). Both systems indicated overall wet conditions over East Africa (Figs. 5e–g,i–k). However the SEAS5 ensemble overwhelmingly forecast a large wet event, raising the probability of an upper quintile event (80th percentile, 1 in 5 years) to over 50% across the region, and over 70% in some places (Fig. 5g). However as shown by CHIRPS observations (Fig. 5c), the region actually experiencing an upper quintile rainfall event was restricted to Uganda, southern Kenya, and a small part of Somalia and Ethiopia. SEAS5 did not capture the spatial variability in the event and instead indicated strong wet anomalies across the entire East African region, in a similar way to the pattern observed in 1997. GloSea5 also indicated increased probabilities of such a wet event to occur, with a higher probability of an upper quintile event to occur over Uganda, southern Somalia, western Kenya, and most of Tanzania and normal probabilities shown in the Mandera triangle region; however, the spatial pattern of GloSea5 anomalies are more consistent with observations, while the probabilities of an upper quintile event were lower than SEAS5.

Observed and predicted sea surface temperature anomalies are also shown in Figs. 5c, 5f, and 5i. HadISST observed anomalies depict the strong El Niño event in the Pacific and warming across the Indian Ocean. Warm anomalies are observed in the western Indian Ocean, with normal conditions in the eastern part, corresponding to a positive IOD event. Ensemble mean anomalies from the two forecast systems indicate a realistic representation of the spatial pattern of warming in the Pacific, including the warm blob off the coasts of California (Tseng et al. 2017). However though both systems captured the warming in the west Indian Ocean, the SEAS5 ensemble overestimates the zonal SST gradient across the basin and simulated cold anomalies of -1 K in the east Indian Ocean with generally cold conditions across the Maritime Continent. By contrast, the GloSea5 ensemble mean SST anomalies in the east were more closely aligned with observations.

These results are consistent with Black et al. (2003), who demonstrated that extreme rainfall over East Africa only occurs when the zonal SST gradient over the Indian Ocean reverses for several months. To look in more detail within the SEAS5 ensemble, anomalies predicted by individual ensemble members are shown in Figs. S2–S5. For precipitation nearly all members indicate wet anomalies, although it should be noted that at least one ensemble members is as dry as the observations, so the actual outcome did fall within the range of the forecast ensemble (Fig. S2). Circulation patterns are shown as departures from the ensemble mean in Figs. S3 and S4 for zonal wind at 850 and 200 mb. There is no

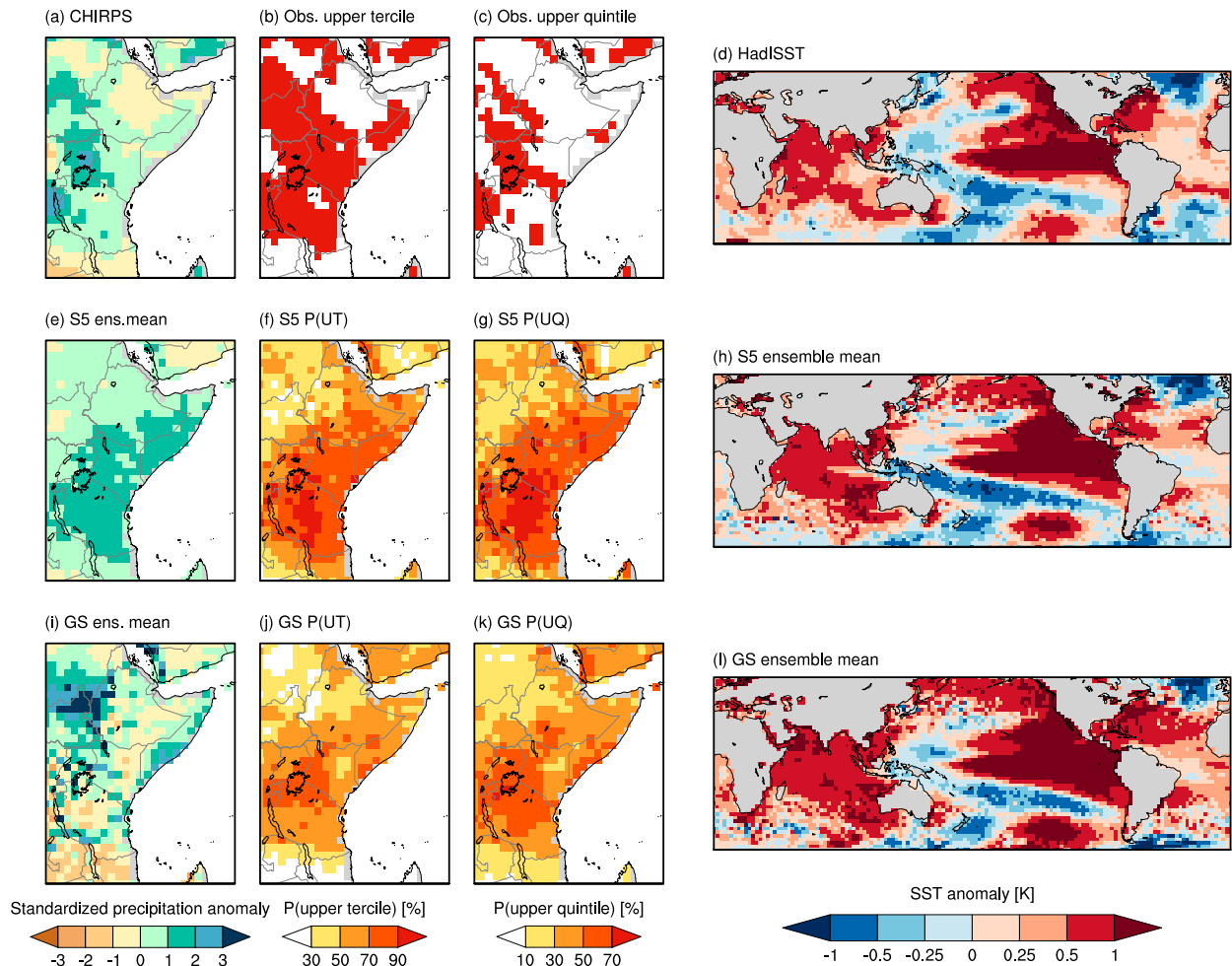


FIG. 5. OND 2015 precipitation and SST in (top) observations, (middle) SEAS5, and (bottom) GloSea5. (a),(e),(i) Standardized OND precipitation anomalies in CHIRPS and the ensemble mean from the two systems. Regions where OND rainfall was in the upper (b),(f),(j) tercile and (c),(g),(k) quintile, in CHIRPS in (b) and (c), and the forecast probabilities for those events in the two forecast systems in (f),(g),(j), and (k); note the different color scale. (right) OND SST anomalies in HadISST in (d) and the ensemble mean SST anomaly in SEAS5 and GloSea5 in (h) and (l).

clear systematic relationship within the ensemble between circulation and precipitation: there is a slight tendency for wetter members to have easterly (negative zonal wind) anomalies at 850 mb near the Kenya coast, consistent with the interannual relationship with the Indian Ocean Walker circulation, but this is not apparent for all members. For instance, the very wettest member also has the most westerly winds in the west Indian Ocean.

However, analysis of the SST anomalies predicted by the ensemble (Fig. S5) reveals that all members have a similar distinct “cold tongue” in the Indian Ocean, consisting of relatively sharp meridional gradients. This cold tongue stretches out from Indonesia into the central Indian Ocean and is visible in the ensemble mean, but is not present in the observed SST (Fig. 5); all SEAS5 ensemble members predict sharper meridional gradients than

observed. This suggests a systematic error in the east Indian Ocean and tendency to overestimate the chance of a positive IOD in the Indian Ocean given an El Niño in the Pacific, along with errors in the spatial structure of SST anomalies in the east Indian Ocean. It is hypothesized that this bias was largely responsible for the large positive precipitation anomaly forecast over East Africa. Seasonal forecast relaxation experiments have then been carried out to test this hypothesis and results are described in the next section.

c. Relaxation experiments to investigate the source of the strong wet signal in SEAS5

The impact of the relaxation experiments on simulated OND 2015 conditions relative to the control experiment is shown in Fig. 6 (for reference the mean and

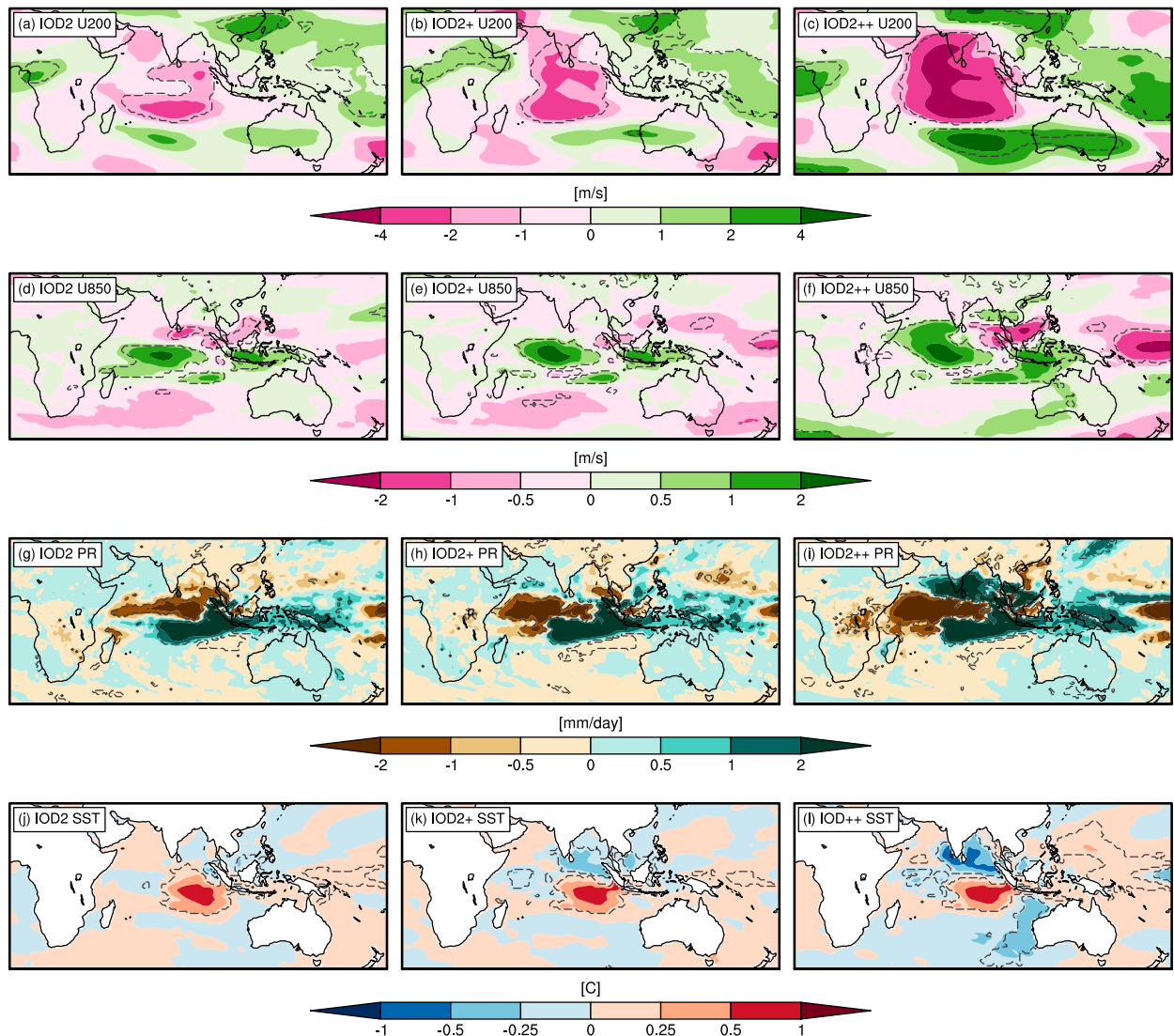


FIG. 6. Results from the relaxation experiments for reforecasts of OND 2015. Differences of the mean of each experiment 25-member ensemble against the mean of the 25-member control ensemble run are shown for (a)–(c) zonal wind at 200 mb, (d)–(f) zonal wind at 850 mb, (g)–(i) precipitation, and (j)–(l) SST. Results for the three experiments (left) IOD2, (center) IOD2+, and (right) IOD2++ are shown. In each case differences between the means of the two ensembles that are significant at the 99% level based on a two-sided t test are indicated by a dashed gray contour line.

anomalies for each experiment are shown in Figs. S6 and S7). All three experiments that relax the atmosphere toward reanalyses over the eastern Indian Ocean lead to a reduction in the simulated cold SST anomaly there compared to the control (Figs. 6j–l). However, the magnitude of the impact on dynamics outside of this region depends on the extent of the relaxation box used.

In the IOD2 experiment some impact is seen on the zonal wind fields (Figs. 6a,d). Equatorial easterly anomalies at 850 mb are reduced in the central Indian Ocean, while the easterly anomalies at 200 mb south of the equator are reduced. This leads to a drier

precipitation signal in the western Indian Ocean and a wetter signal in the east (Fig. 6g), consistent with a smaller westward extension of the surface zonal wind anomalies and a more eastward location of convergent winds. However, no significant impact is seen on the continental precipitation signal over East Africa.

By extending the relaxation box to the central Indian Ocean (experiment IOD2+), a larger impact on the precipitation signal over the Indian Ocean is shown (Fig. 6h), while the impact on zonal winds at 850 mb is slightly higher and the impact on the winds at 200 mb extends to a larger region (Figs. 6b,e). However no significant difference in

the precipitation signal over East Africa is seen in the IOD2+ experiment either (Fig. 6h).

Only the IOD2++ experiment shows widespread significant drying of the precipitation signal over East Africa with respect to the control (Fig. 6i). This is accompanied by a larger impact on the wind anomalies at 200 mb compared to the IOD1 and IOD2+ experiments and a slightly larger extent of impact on the zonal wind fields at 850 mb (Figs. 6c,f). Outside of East Africa, the impact of this experiment on precipitation leads to a strong drying signal all across the western Indian Ocean, extending into the east, with significant wetting north and south of the dry signal. The IOD2++ experiment also leads to a cooling of the equatorial Pacific in the Niño region, demonstrating that the link between ENSO and the Indian Ocean is not a one-way forcing; the Indian Ocean has the potential to moderate El Niño events.

The rainfall reduction over the East Africa is only apparent for the IOD2++ experiment, which extends the relaxation box across the eastern Indian Ocean. This suggests that model errors are not confined to the traditional spatial domain used to define the eastern pole of the IOD; rather, coupled near-surface processes in the Indian Ocean west of 70°E and both sides of the equator are important. This reduction is in the wet signal over the Indian Ocean across the experiments is proportional to the size of the impact on winds at both 850 and 200 mb, with larger reductions coincident with a reduction in the size of near-surface easterly anomalies and an increase in the size of westerly anomalies at height, consistent with a weaker reduction in the strength of the Walker-type circulation in the relaxation experiments.

Specifically, a tendency toward too-cold SST anomalies in SEAS5 for 2015 led to a reduction in convection over the Maritime Continent, leading to both reduced convergence at the surface and divergence aloft. These simultaneously led to a reduction in the strength of the Walker-type circulation over the Indian Ocean, thereby increasing the wet signal over East Africa through reduced moisture flux away from the continent at the surface and enhanced potential for deep convection through reduced convergence aloft. The accompaniment of the strong reduction in the East Africa dry signal in the IOD2++ experiment by a particularly strong increase in the impact on the zonal wind at 200 mb points in particular to the upper branch of the Indian Ocean walker cell as a key player in modulating the impacts of the 2015 El Niño on East African rainfall.

4. Discussion and conclusions

The year 2015 experienced one of the strongest El Niños on record, and the humanitarian preparedness response was based largely on impacts observed during previous

large El Niño events. However, although some parts of East Africa experienced a particularly wet season, for most regions the wet anomaly was not particularly large and some parts even experienced a drier than average season. This was due to a positive but weaker IOD phase compared to previous El Niño events (such as the 1997 event) and led to a smaller reduction in the strength of the Indian Ocean Walker-type circulation.

Seasonal forecasts well anticipated the strong El Niño event of 2015, but at 1-month lead the operational ECMWF SEAS5 reforecast indicated large probabilities of an extreme wet season that did not happen in many regions, along with a too-strong zonal SST gradient in the Indo-Pacific basin. In addition systematic errors were found in the structure of SST anomalies in the East Indian Ocean in the reforecast ensemble, where sharp meridional gradients of SST were present in every ensemble member but not seen in observations.

Relaxation experiments confirm that atmosphere–ocean processes below 700 mb over the eastern Indian Ocean were a key driver of the high SEAS5 forecast probabilities for wet conditions. By nudging the atmosphere in this region toward observations the model simulates a weaker reversal of the Walker cell and reproduces a more realistic drier signal over East Africa in 2015. Interestingly, the experiment that leads to drying over East Africa also shows widespread significant impacts on the zonal wind fields at 200 mb, suggesting that the upper branch of the cell and associated impacts on upper-tropospheric divergence were a key factor in the 2015 event over East Africa. Further work to explore this link might consider additional relaxation experiments where a region is relaxed to an alternative year. For example, a reforecast of 1997 could relax the East Indian Ocean to 2015, to see to what extent activity here would modify the wet signal over East Africa. Another alternative would be atmosphere-only forced-SST initialized seasonal reforecasts to test the sensitivity of East African rainfall to the magnitude and position of SST anomalies in the east Indian Ocean.

Work to understand the unexpectedly moderate response of the southwestern United States to the 2015/16 El Niño has suggested that response was related to internal atmospheric variability. In particular [Zhang et al. \(2018\)](#) suggest a particularly active Madden–Julian oscillation (MJO) during the season was an important factor. However MJO activity is unable to explain the moderate response over East Africa, where an active MJO in phases 2–4 is normally associated with particularly wet periods ([Berhane and Zaitchik 2014](#); [Zaitchik 2017](#)). MJO activity over OND 1997 and 2015 (Fig. S8) shows an inactive MJO in 1997 whereas 2015 had MJO particularly in phases 2–4 in 2015. Given this alone one would expect 2015 to be wetter than 1997.

However, despite clear differences between East African and western U.S. climate, results may be compared the work of Siler et al. (2017), who linked the dry conditions over the western United States to a dipole pattern of SST variability across the Indian Ocean and west Pacific, a pattern resembling the IOD. This pattern of SST variability was not well captured by seasonal forecasts from the North American Multimodel Ensemble, which had erroneous predictions of above-average precipitation in the western United States. The Indian Ocean response to the 2015 El Niño and the inability of most seasonal forecast models to capture the SST pattern corresponding to a mild IOD may have then impacted East Africa in addition to the western United States.

The impact of strong IOD events on East African climate has been demonstrated previously: IOD events that reverse the zonal SST gradient over the Indian basin for several months trigger extreme rainfall over the region (Black et al. 2003). Although IOD events are often triggered by Pacific ENSO they can also occur independently (Schott et al. 2009). However, a study of preparedness responses during 2015 indicated that humanitarian actors solely based actions on the impacts of a similar intensity El Niño and did not consider the state of the Indian Ocean at all (Tozier de la Poterie et al. 2018).

The implication of these results for the humanitarian sector working in East Africa is that they should not rely on ENSO outlooks in isolation to guide preparedness actions, and should not assume that the impacts of the next El Niño will be similar to former events. The state of the Indian Ocean is also critical in modulating East African short rains, the IOD in particular. The output of coupled climate model forecasts has the potential to provide more accurate warnings than an “analog year” approach to early intervention; however, a close examination of predictability and model skill is necessary if forecasts are to be relied upon (Kilavi et al. 2018).

It is important to note that the SEAS5 increased probabilities of an extreme wet season were not necessarily “wrong”: strictly, it is impossible to say if a single probabilistic forecast is wrong or right (as long as 0% or 100% probabilities are not issued). In 2015, over most of the region the SEAS5 probability that the rainfall would be above the upper quintile was around 50%; this corresponds to a probability of around 50% that the rainfall will *not* be above the upper quintile. Indeed, looking at all 25 individual SEAS5 ensemble members over East Africa shows at least one member as dry as the observations (Fig. S2). That is, although the SEAS5 ensemble overall had a strong wet signal, the verification observations still fall within the range of possible futures estimated by the model. In addition, it should be made

clear that this research considers a particular “edge case” rather than overall seasonal forecast performance. This has been assessed across the whole SEAS5 hindcast, demonstrating that in general SEAS5 performs particularly well the East African short rains [see MacLeod (2019a,b) for further details].

However, the results here lead to the hypothesis that SEAS5 has a systematic bias toward strong positive IOD events during strong El Niños. This is consistent with previous work showing a significant overestimation of the correlation between Indian Ocean and Pacific rainfall anomalies (Molteni et al. 2015). With only a small sample of strong El Niño events in the seasonal reforecast period it is difficult to make a robust claim of this link. Future work will look at 110-yr experimental reforecast of the ECMWF seasonal prediction system [a coupled version of that system is described in Weisheimer et al. (2017)], which may shed further light on this question. This will help to better understand the behavior of state-of-the-art coupled climate models in order to improve rainfall predictions over East Africa.

Acknowledgments. DM is supported by the NERC/DfID project ForPac: Toward Forecast-based Preparedness Action (NE/P000673/1). CC was funded by the NERC project “Impact of El Niño on malaria vector dynamics in Tanzania: Observation, improvement and unleashing forecasting potential” (NE/P004407/1) as well as by the National Institute for Health Research Health Protection Research Unit in Emerging and Zoonotic Infections at the University of Liverpool in partnership with Public Health England and Liverpool School of Tropical Medicine. The views expressed are those of the authors and not necessarily those of the NHS, the NIHR, the Department of Health, or Public Health England. Reforecast and reanalysis data were downloaded from the Copernicus Data Store, CHIRPS data from the Climate Hazards Group of UCSB, and climate model experiments were carried out using a member state special project at ECMWF, where data are archived (details available on request).

REFERENCES

- Adler, R. F., and Coauthors, 2003: The version-2 Global Precipitation Climatology Project (GPCP) monthly precipitation analysis (1979–present). *J. Hydrometeorol.*, **4**, 1147–1167, [https://doi.org/10.1175/1525-7541\(2003\)004<1147:TVGPCP>2.0.CO;2](https://doi.org/10.1175/1525-7541(2003)004<1147:TVGPCP>2.0.CO;2).
- Anyamba, A., and Coauthors, 2019: Global disease outbreaks associated with the 2015–2016 El Niño event. *Sci. Rep.*, **9**, 1930, <https://doi.org/10.1038/s41598-018-38034-z>.
- Berhane, F., and B. Zaitchik, 2014: Modulation of daily precipitation over East Africa by the Madden–Julian oscillation. *J. Climate*, **27**, 6016–6034, <https://doi.org/10.1175/JCLI-D-13-00693.1>.

- Black, E., 2005: The relationship between Indian Ocean sea-surface temperature and East African rainfall. *Philos. Trans. Roy. Soc.*, **363A**, 43–47, <https://doi.org/10.1098/RSTA.2004.1474>.
- , J. Slingo, and K. R. Sperber, 2003: An observational study of the relationship between excessively strong short rains in coastal East Africa and Indian Ocean SST. *Mon. Wea. Rev.*, **131**, 74–94, [https://doi.org/10.1175/1520-0493\(2003\)131<0074:AOSOTR>2.0.CO;2](https://doi.org/10.1175/1520-0493(2003)131<0074:AOSOTR>2.0.CO;2).
- Brown, V., M. Abdir Issak, M. Rossi, P. Barboza, and A. Paugam, 1998: Epidemic of malaria in north-eastern Kenya. *Lancet*, **352**, 1356–1357, [https://doi.org/10.1016/S0140-6736\(05\)60747-7](https://doi.org/10.1016/S0140-6736(05)60747-7).
- Caminade, C., J. Turner, S. Metelmann, J. C. Hesson, M. S. C. Blagrove, T. Solomon, A. P. Morse, and M. Baylis, 2017: Global risk model for vector-borne transmission of Zika virus reveals the role of El Niño 2015. *Proc. Natl. Acad. Sci. USA*, **114**, 119–124, <https://doi.org/10.1073/pnas.1614303114>.
- Cash, B. A., and N. J. Burls, 2019: Predictable and unpredictable aspects of U.S. West Coast rainfall and El Niño: Understanding the 2015/16 event. *J. Climate*, **32**, 2843–2868, <https://doi.org/10.1175/JCLI-D-18-0181.1>.
- Chretien, J.-P., A. Anyamba, J. Small, S. Britch, J. L. Sanchez, A. C. Halbach, C. Tucker, and K. J. Linthicum, 2015: Global climate anomalies and potential infectious disease risks: 2014–2015. *PLOS Currents Outbreaks*, **1**, <https://doi.org/10.1371/currents.outbreaks.95fbc4a8fb4695e049baabfc2fc8289f>.
- Claar, D. C., L. Szostek, J. M. McDevitt-Irwin, J. J. Schanze, and J. K. Baum, 2018: Global patterns and impacts of El Niño events on coral reefs: A meta-analysis. *PLOS ONE*, **13**, e0190957, <https://doi.org/10.1371/journal.pone.0190957>.
- Dee, D. P., and Coauthors, 2011: The ERA-Interim reanalysis: Configuration and performance of the data assimilation system. *Quart. J. Roy. Meteor. Soc.*, **137**, 553–597, <https://doi.org/10.1002/qj.828>.
- Emerton, R., H. L. Cloke, E. M. Stephens, E. Zsoter, S. J. Woolnough, and F. Pappenberger, 2017: Complex picture for likelihood of ENSO-driven flood hazard. *Nat. Commun.*, **8**, 14796, <https://doi.org/10.1038/ncomms14796>.
- Field, R. D., and Coauthors, 2016: Indonesian fire activity and smoke pollution in 2015 show persistent nonlinear sensitivity to El Niño-induced drought. *Proc. Natl. Acad. Sci. USA*, **113**, 9204–9209, <https://doi.org/10.1073/pnas.1524888113>.
- Fontaine, R. E., A. E. Najjar, and J. S. Prince, 1961: The 1958 malaria epidemic in Ethiopia. *Amer. J. Trop. Med. Hyg.*, **10**, 795–803, <https://doi.org/10.4269/ajtmh.1961.10.795>.
- Funk, C., and Coauthors, 2015: The Climate Hazards Infrared Precipitation with Stations—A new environmental record for monitoring extremes. *Sci. Data*, **2**, 150066, <https://doi.org/10.1038/sdata.2015.66>.
- Hales, S., P. Weinstein, Y. Souares, and A. Woodward, 1999: El Niño and the dynamics of vectorborne disease transmission. *Environ. Health Perspect.*, **107**, 99–102, <https://doi.org/10.1289/EHP.9910799>.
- Hastenrath, S., A. Nicklis, and L. Greischar, 1993: Atmospheric-hydrospheric mechanisms of climate anomalies in the western equatorial Indian Ocean. *J. Geophys. Res.*, **98**, 20 219–20 235, <https://doi.org/10.1029/93JC02330>.
- , D. Polzin, and C. Mutai, 2011: Circulation mechanisms of Kenya rainfall anomalies. *J. Climate*, **24**, 404–412, <https://doi.org/10.1175/2010JCLI3599.1>.
- Huang, B., M. L'Heureux, Z.-Z. Hu, and H.-M. Zhang, 2016: Ranking the strongest ENSO events while incorporating SST uncertainty. *Geophys. Res. Lett.*, **43**, 9165–9172, <https://doi.org/10.1002/2016GL070888>.
- ICPAC, 2015: Statement from the 41st Greater Horn of Africa Climate Outlook Forum. Dar es Salaam, Tanzania, IGAD Climate Prediction and Applications Centre (ICPAC), 3 pp., <https://perma.cc/9C2X-PHRU>.
- Indeje, M., F. H. Semazzi, and L. J. Ogallo, 2000: ENSO signals in East African rainfall seasons. *Int. J. Climatol.*, **20**, 19–46, [https://doi.org/10.1002/\(SICI\)1097-0088\(200001\)20:1<19::AID-JOC449>3.0.CO;2-0](https://doi.org/10.1002/(SICI)1097-0088(200001)20:1<19::AID-JOC449>3.0.CO;2-0).
- Ineson, S., and Coauthors, 2018: Predicting El Niño in 2014 and 2015. *Sci. Rep.*, **8**, 10733, <https://doi.org/10.1038/s41598-018-29130-1>.
- International Federation of Red Cross and Red Crescent Societies, 2017: Emergency Plan of Action update—Ethiopia: Drought. IFRC, 15 pp., <http://adore.ifrc.org/Download.aspx?FileId=156069>.
- Jung, T., 2011: Diagnosing remote origins of forecast error: Relaxation versus 4D-Var data-assimilation experiments. *Quart. J. Roy. Meteor. Soc.*, **137**, 598–606, <https://doi.org/10.1002/qj.781>.
- Kilavi, M., and Coauthors, 2018: Extreme rainfall and flooding over central Kenya including Nairobi City during the long-rains season 2018: Causes, predictability, and potential for early warning and actions. *Atmosphere*, **9**, 472, <https://doi.org/10.3390/atmos9120472>.
- Kilian, A., P. Langi, A. Talisuna, and G. Kabagambe, 1999: Rainfall pattern, El Niño and malaria in Uganda. *Trans. Roy. Soc. Trop. Med. Hyg.*, **93**, 22–23, [https://doi.org/10.1016/S0035-9203\(99\)90165-7](https://doi.org/10.1016/S0035-9203(99)90165-7).
- Kovats, R. S., M. J. Bouma, S. Hajat, E. Worrall, and A. Haines, 2003: El Niño and health. *Lancet*, **362**, 1481–1489, [https://doi.org/10.1016/S0140-6736\(03\)14695-8](https://doi.org/10.1016/S0140-6736(03)14695-8).
- L'Heureux, M. L., and Coauthors, 2017: Observing and predicting the 2015/16 El Niño. *Bull. Amer. Meteor. Soc.*, **98**, 1363–1382, <https://doi.org/10.1175/BAMS-D-16-0009.1>.
- Lim, Y.-K., S. D. Schubert, Y. Chang, A. M. Molod, and S. Pawson, 2018: The impact of SST-forced and unforced teleconnections on 2015/16 El Niño winter precipitation over the western United States. *J. Climate*, **31**, 5825–5844, <https://doi.org/10.1175/JCLI-D-17-0218.1>.
- MacLachlan, C., and Coauthors, 2015: Global Seasonal forecast system version 5 (GloSea5): A high-resolution seasonal forecast system. *Quart. J. Roy. Meteor. Soc.*, **141**, 1072–1084, <https://doi.org/10.1002/qj.2396>.
- MacLeod, D., 2019a: Seasonal forecast skill over the Greater Horn of Africa: A verification atlas of System 4 and SEAS5. Part 1: Precipitation. ECMWF Tech. rep., 69 pp., <https://www.ecmwf.int/node/18906>.
- , 2019b: Seasonal forecast skill over the Greater Horn of Africa: A verification atlas of System 4 and SEAS5. Part 2: 2-m temperature. ECMWF Tech. Rep., 75 pp., <https://www.ecmwf.int/node/18923>.
- Mason, S. J., and L. Goddard, 2001: Probabilistic precipitation anomalies associated with ENSO. *Bull. Amer. Meteor. Soc.*, **82**, 619–638, [https://doi.org/10.1175/1520-0477\(2001\)082<0619:PPAAWE>2.3.CO;2](https://doi.org/10.1175/1520-0477(2001)082<0619:PPAAWE>2.3.CO;2).
- , and C. Simbarashe, 2009: IRI Position paper: Verification of African RCOF forecasts. IRI Tech. Rep. 09-02, 24 pp., <https://doi.org/10.7916/D85T3SB0>.
- McGregor, G., and K. Ebi, 2018: El Niño Southern Oscillation (ENSO) and health: An overview for climate and health researchers. *Atmosphere*, **9**, 282, <https://doi.org/10.3390/atmos9070282>.
- McPhaden, M. J., S. E. Zebiak, and M. H. Glantz, 2006: ENSO as an integrating concept in Earth science. *Science*, **314**, 1740–1745, <https://doi.org/10.1126/science.1132588>.

- Molteni, F., T. N. Stockdale, and F. Vitart, 2015: Understanding and modelling extra-tropical teleconnections with the Indo-Pacific region during the northern winter. *Climate Dyn.*, **45**, 3119–3140, <https://doi.org/10.1007/s00382-015-2528-y>.
- Muñoz, Á. G., M. C. Thomson, A. M. Stewart-Ibarra, G. A. Vecchi, X. Chourio, P. Nájera, Z. Moran, and X. Yang, 2017: Could the recent Zika epidemic have been predicted? *Front. Microbiol.*, **8**, 1291, <https://doi.org/10.3389/fmicb.2017.01291>.
- Mutai, C. C., and M. N. Ward, 2000: East African rainfall and the tropical circulation/convection on intraseasonal to interannual timescales. *J. Climate*, **13**, 3915–3939, [https://doi.org/10.1175/1520-0442\(2000\)013<3915:EARATT>2.0.CO;2](https://doi.org/10.1175/1520-0442(2000)013<3915:EARATT>2.0.CO;2).
- Nicholson, S. E., 2017: Climate and climatic variability of rainfall over eastern Africa. *Rev. Geophys.*, **55**, 590–635, <https://doi.org/10.1002/2016RG000544>.
- Omumbo, J. A., B. Lyon, S. M. Waweru, S. J. Connor, and M. C. Thomson, 2011: Raised temperatures over the Kericho tea estates: Revisiting the climate in the East African highlands malaria debate. *Malar. J.*, **10**, 12, <https://doi.org/10.1186/1475-2875-10-12>.
- Quan, X.-W., M. Hoerling, L. Smith, J. Perlwitz, T. Zhang, A. Hoell, K. Wolter, and J. Eischeid, 2018: Extreme California rains during winter 2015/16: A change in El Niño teleconnection? *Bull. Amer. Meteor. Soc.*, **99**, S49–S53, <https://doi.org/10.1175/BAMS-D-17-0118.1>.
- Rayner, N. A., D. E. Parker, E. B. Horton, C. K. Folland, L. V. Alexander, D. P. Rowell, E. C. Kent, and A. Kaplan, 2003: Global analyses of sea surface temperature, sea ice, and night marine air temperature since the late nineteenth century. *J. Geophys. Res.*, **108**, 4407, <https://doi.org/10.1029/2002JD002670>.
- Saji, N. H., B. N. Goswami, P. N. Vinayachandran, and T. Yamagata, 1999: A dipole mode in the tropical Indian Ocean. *Nature*, **401**, 360–363, <https://doi.org/10.1038/43854>.
- Schott, F. A., S.-P. Xie, and J. P. McCreary, 2009: Indian Ocean circulation and climate variability. *Rev. Geophys.*, **47**, RG1002, <https://doi.org/10.1029/2007RG000245>.
- Siler, N., Y. Kosaka, S. P. Xie, and X. Li, 2017: Tropical ocean contributions to California's surprisingly dry El Niño of 2015/16. *J. Climate*, **30**, 10 067–10 079, <https://doi.org/10.1175/JCLI-D-17-0177.1>.
- Sorensen, C. J., M. J. Borbor-Cordova, E. Calvellido-Hynes, A. Diaz, J. Lemery, and A. M. Stewart-Ibarra, 2017: Climate variability, vulnerability, and natural disasters: A case study of Zika virus in Manabí, Ecuador following the 2016 earthquake. *GeoHealth*, **1**, 298–304, <https://doi.org/10.1002/2017GH000104>.
- Tozier de la Poterie, A. S., W. E. Jemba, R. Singh, E. Coughlan de Perez, C. V. Costella, and J. Arrighi, 2018: Understanding the use of 2015–2016 El Niño forecasts in shaping early humanitarian action in eastern and southern Africa. *Int. J. Disaster Risk Reduct.*, **30**, 81–94, <https://doi.org/10.1016/j.ijdr.2018.02.025>.
- Tseng, Y.-H., R. Ding, and X.-M. Huang, 2017: The warm Blob in the northeast Pacific—The bridge leading to the 2015/16 El Niño. *Environ. Res. Lett.*, **12**, 054019, <https://doi.org/10.1088/1748-9326/aa67c3>.
- Vicente-Serrano, S. M., J. I. López-Moreno, L. Gimeno, R. Nieto, E. Morán-Tejeda, J. Lorenzo-Lacruz, S. Beguería, and C. Azorin-Molina, 2011: A multiscale global evaluation of the impact of ENSO on droughts. *J. Geophys. Res.*, **116**, D20109, <https://doi.org/10.1029/2011JD016039>.
- Wanders, N., and Coauthors, 2017: Forecasting the hydroclimatic signature of the 2015/16 El Niño event on the western United States. *J. Hydrometeorol.*, **18**, 177–186, <https://doi.org/10.1175/JHM-D-16-0230.1>.
- Weisheimer, A., N. Schaller, C. O'Reilly, D. A. MacLeod, and T. Palmer, 2017: Atmospheric seasonal forecasts of the twentieth century: Multi-decadal variability in predictive skill of the winter North Atlantic Oscillation (NAO) and their potential value for extreme event attribution. *Quart. J. Roy. Meteor. Soc.*, **143**, 917–926, <https://doi.org/10.1002/QJ.2976>.
- Wolff, C., G. H. Haug, A. Timmermann, J. S. S. Damste, A. Brauer, D. M. Sigman, M. A. Cane, and D. Verschuren, 2011: Reduced interannual rainfall variability in East Africa during the last Ice Age. *Science*, **333**, 743–747, <https://doi.org/10.1126/science.1203724>.
- Zaitchik, B. F., 2017: Madden–Julian oscillation impacts on tropical African precipitation. *Atmos. Res.*, **184**, 88–102, <https://doi.org/10.1016/j.atmosres.2016.10.002>.
- Zhang, T., and Coauthors, 2018: Predictability and prediction of Southern California rains during strong El Niño events: A focus on the failed 2016 winter rains. *J. Climate*, **31**, 555–574, <https://doi.org/10.1175/JCLI-D-17-0396.1>.